

中国激光

高速激光熔覆铁基合金涂层的组织及性能研究

徐一飞¹, 孙耀宁^{1*}, 王国建¹, 贵永亮²

¹ 新疆大学机械工程学院, 新疆 乌鲁木齐 830047;

² 华北理工大学冶金与能源学院, 河北 唐山 063210

摘要 针对综采工作面典型零件防护涂层快速修复和制造的需要, 本文以取代传统镀铬工艺为目标, 采用高速激光熔覆在 45 钢表面制备了高质量的铁基合金涂层。采用超景深三维显微系统观察涂层的表面形貌, 采用光学显微镜、扫描电镜及能谱分析仪研究了熔覆层的显微形貌及元素含量变化, 采用 X 射线衍射技术分析了涂层各部分的物相组成, 利用显微硬度计测试了涂层的显微硬度, 最后采用电化学工作站测试了涂层的耐蚀性。结果表明: 高速激光熔覆的熔覆效率为 $0.243 \text{ m}^2/\text{h}$; 涂层平整均匀, 表面粗糙度 $R_a \approx 21.38 \mu\text{m}$; 涂层组织均匀致密, 且与基体实现了良好的冶金结合, 稀释率约为 7.1%; 涂层主要由铁素体和奥氏体组成, 晶粒细密, 平均晶粒直径不超过 $2.8 \mu\text{m}$; 涂层表面的显微硬度约为基体的 3 倍; 涂层的自腐蚀电流密度为基体的 0.33%, 其优异的耐蚀性源于更均匀的成分分布。

关键词 激光技术; 高速激光熔覆; 铁基合金; 电镀铬; 耐蚀涂层

中图分类号 TG174.4 文献标志码 A

doi: 10.3788/CJL202148.1002122

1 引言

新疆作为我国乃至全球重要的矿域之一, 煤炭预测储量高达 21900 亿吨, 占全国预测储量的四成以上。随着《丝绸之路经济带核心区能源规划》^[1]的发布, 新疆煤炭工业即将迈入前所未有的大跃进式发展。电镀铬工艺被广泛应用于综采工作面液压支架气缸、活塞杆等典型零部件的表面防护, 该工艺巨大的耗电量使得利润空间一再被压缩, 这一问题与电镀废气、废液引起的污染问题是制约新疆煤炭工业实现环境友好型发展的难题。激光熔覆技术是硬铬电镀的主要替代工艺之一, 该工艺虽然具有结合强度高、工件变形小等优点^[2-3], 但却因成本较高(约为电镀工艺的 6 倍^[4])而无法被广泛投放市场。

2013 年, 德国弗劳恩霍夫激光技术研究所 (Fraunhofer ILT) 的 Raykis^[5]联合亚琛工业大学 (RWTH-Aachen) 基于激光熔覆技术提出了超高速激光熔覆 (EHLA) 技术, 该技术的最高速度可达到

200 m/min , 这意味着可以实现 $500 \text{ cm}^2/\text{min}$ 的生产效率^[7], 可在大幅提高生产效率的同时保证表面成形精度, 并可降低后续加工制造成本, 为替代电镀铬涂层工艺的开发提供了新思路和新方法。目前的相关研究主要集中于超高速专用装置及粉末研发、温度场和熔池行为仿真、超高速工艺、组织与性能优化等方面。如: 西安交通大学的王豫跃等^[8]制备出了具有自主知识产权的系列超高速激光熔覆装备; 瑞典的 Höganäs AB 以及瑞士的 Oerlikon Metco 公司得出了超高速激光熔覆涂层厚度 t 与送粉率 G 、激光功率 P 、搭接率 O 的函数关系式, 即 $t = nG/[P(100-O)]^{[9]}$, 其中 n 为大于 0 的自然数; 哈尔滨工业大学的李俐群等^[10]在调质处理的 27SiMn 液压支架基材上成功制备了涂层致密、成分均匀、热影响区窄、稀释率小、耐蚀性优异的 431 不锈钢耐蚀涂层; Lampa 等^[9]应用超高速激光熔覆工艺制备了由质量分数为 18% 的铬和质量分数为 2.5% 的铌组成的新型铁基合金涂层, 该涂层具有良好的耐磨性

收稿日期: 2020-08-14; 修回日期: 2020-08-19; 录用日期: 2020-10-26

基金项目: 新疆维吾尔自治区自然科学基金 (2020D01C030)、河北省杰出青年科学基金 (E2019209473)、河北省高校百名优秀创新人才支持计划 (III) (SLRC2019030)

* E-mail: 1327195386@qq.com

和耐蚀性;李岩等^[11]利用快速激光熔覆技术在 45 钢基体上制备了铁基合金涂层,分析了高速激光熔覆涂层的表面形貌与微观结构,并表征了涂层的表面粗糙度与显微硬度。目前,大部分针对高速激光熔覆的研究还处于参数化研究和数据摸索阶段。

高速激光熔覆工作原理、传热模式的变化导致其制备的涂层的宏观特征、微观组织及耐蚀性都有所不同。为了了解微观组织在高速激光熔覆工艺的极速热循环过程中的演变规律,并实现力学性能的调控^[12],本文以煤矿产业液压支柱常用的 45 钢(GB/T 17396—1998^[13])为基体材料,利用高速激光熔覆技术通过多道搭接连续制备了大面积铁基合金涂层,然后对涂层的宏观形貌、显微组织、硬度、耐蚀性进行分析,为提高液压支柱的耐蚀性与使用寿命提供实验依据。

2 实验材料与方法

2.1 原材料选择

基体选用尺寸为 $100 \text{ mm} \times 60 \text{ mm} \times 10 \text{ mm}$ 的 45 钢板材,熔覆材料为铁基合金粉末,其粒径为

表 2 激光熔覆工艺参数

Table 2 Parameters in laser cladding process

Laser power /W	Scanning velocity / ($\text{mm} \cdot \text{min}^{-1}$)	Powder flow rate / ($\text{r} \cdot \text{min}^{-1}$)	Overlapping rate /%	Cladding efficiency / ($\text{m}^2 \cdot \text{h}^{-1}$)
880	3600	3.0	50	0.243

2.3 高速激光熔覆涂层的测试

采用上海蔡明光学仪器公司生产的 CDM-16C 金相显微镜(OM)观察熔覆层的显微组织,该金相显微镜的最大放大倍数为 1000 倍;采用超景深显微系统测量涂层的表面粗糙度;采用 JSM-7610F Plus 型扫描电子显微镜(SEM)观察熔覆涂层的形貌与微观结构,采用该电镜附带的 X 射线能谱仪(EDS)进行成分分析;采用德国布鲁克 AXS 有限公司生产的 D8 Advance X 射线粉末衍射仪(XRD)进行物相分析,扫描角度 2θ 为 $30^\circ \sim 90^\circ$,步长为 0.02° ;采用 HV-1000 型数字显微硬度计检测试样的显微硬度,加载载荷为 1.96 N,加载时间为 10 s(沿截面厚度方向从距涂层表面 $100 \mu\text{m}$ 处开始测量,每隔 $50 \mu\text{m}$ 测量 3 次,取 3 次测量的算术平均值作为最终的显微硬度值);采用三电极体系的 CHI660E 型电化学工作站测定试样的极化曲线和阻抗曲线,辅助电极为铂电极,参比电极为氯化银电极,开路电位为 $-2.2 \sim 2 \text{ V}$,扫描速率为 0.02 V/s 。

$35 \sim 53 \mu\text{m}$,化学成分如表 1 所示。在进行高速激光熔覆实验前先对基材表面进行清洗,以去除其表面的油污和氧化层,除污去锈的同时可在一定程度上增加表面粗糙度,增加基体对激光的吸收效率。

表 1 铁基合金粉末的化学成分

Table 1 Chemical composition of iron-based alloy powder

Element	C	Si	Cr	Ni	Mo	B	Fe
Mass fraction /%	0.15	4.5	22	13	2	1.6	Bal.

2.2 高速激光熔覆工艺参数

选用西安中科中美激光科技有限公司的 ZKZM-2000 型光纤高速激光器进行高速熔覆实验,激光器的功率范围为 $0 \sim 2200 \text{ W}$,常用光斑直径为 1.2 mm ,离焦量为 15 mm ,采用同轴送粉的方式在 45 钢表面分别熔覆 1~5 层铁基合金粉末,保护气和送粉气均选用体积分数为 99.99% 的氩气。熔覆参数见表 2。在熔覆后的试块上沿垂直于扫描方向采用线切割的方式加工出尺寸为 $8 \text{ mm} \times 8 \text{ mm} \times 8 \text{ mm}$ 的样块,样块经砂纸打磨、抛光后用王水(用 HCl 和 HNO_3 按体积比为 3:1 配制而成)腐蚀制成金相试样,备用。

表 2 激光熔覆工艺参数

Table 2 Parameters in laser cladding process

Laser power /W	Scanning velocity / ($\text{mm} \cdot \text{min}^{-1}$)	Powder flow rate / ($\text{r} \cdot \text{min}^{-1}$)	Overlapping rate /%	Cladding efficiency / ($\text{m}^2 \cdot \text{h}^{-1}$)
880	3600	3.0	50	0.243

3 分析与讨论

3.1 高速激光熔覆涂层的宏观特征

实验得到的熔覆涂层的宏观形貌如图 1 所示。可以看出,熔覆涂层表面连续平整,涂层厚度分别为 $260, 480, 720, 940, 1170 \mu\text{m}$ 。

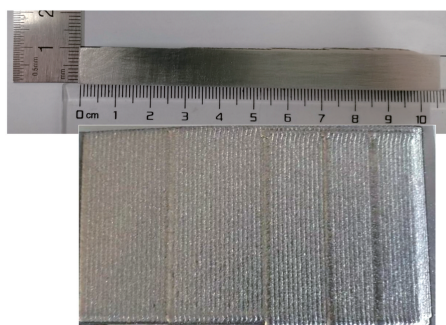


图 1 熔覆涂层的宏观形貌

Fig. 1 Macro morphology of cladding coating

熔覆涂层的表面粗糙度如图 2 所示, R_a 仅为 $21.38 \mu\text{m}$,不足常规激光熔覆涂层的 10%。这主要

是由于高搭接率导致涂层表面波纹起伏减小,仅存少量的未熔粉末颗粒夹杂在表面,如图 3 所示。涂

层的厚度和表面质量决定了加工量和材料利用率,因此高速激光熔覆降低了成品的后加工成本。

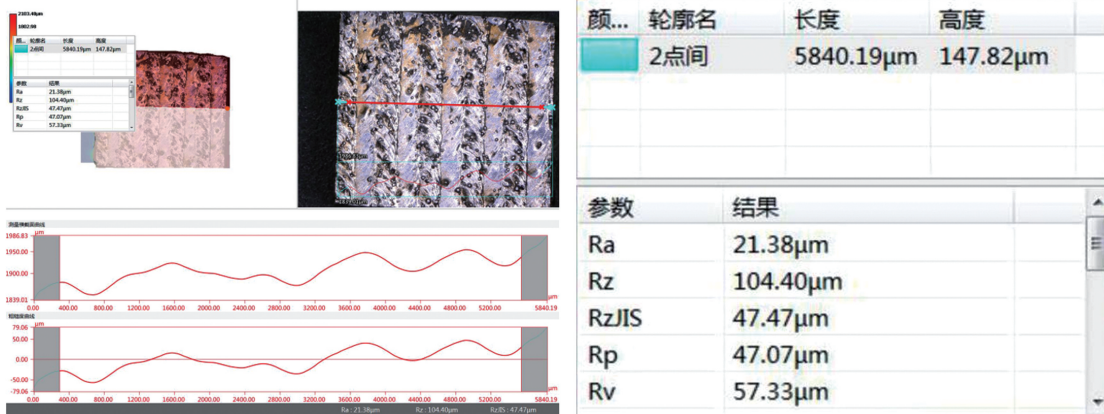


图 2 熔覆涂层的表面粗糙度

Fig. 2 Surface roughness of cladding coating

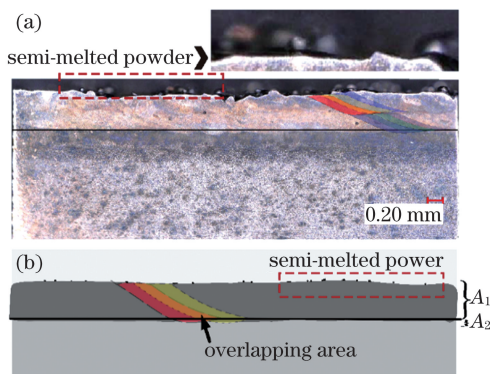


图 3 高速激光熔覆双层涂层的截面形貌。(a)未熔颗粒;(b)稀释率示意图

Fig. 3 Cross-sectional morphologies of double-layer coating.
(a) Unfused particles; (b) schematic of dilution ratio

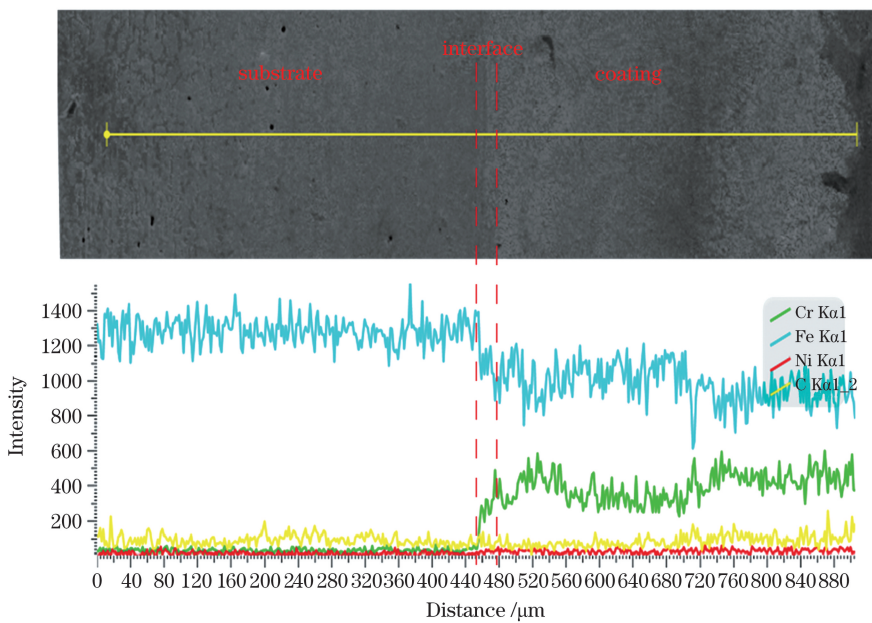


图 4 高速激光熔覆双层涂层的 EDS 分析图谱

Fig. 4 EDS spectrum of high-speed laser cladding double-layer coating

式中: A_1 是熔覆涂层的面积; A_2 是基体的熔化面积。高速激光熔覆制得了单层厚度约为 $260\text{ }\mu\text{m}$ 、稀释率约为 7.1% 的涂层。低稀释率的原因有二:一是高速激光通过调整激光、粉末和熔池的位置,使粉体汇聚于熔池上方,从而使得大部分激光能量用于使熔覆粉末在进入熔池前达到熔融状态,仅有少量激光到达基材产生熔池,这也是高速激光熔覆熔池极小的原因;二是在垂直于高速激光熔覆方向上的多条熔道叠加,导致基体只有一小部分被熔化,并且

这一部分只占整个涂层的一小部分,相当于传统激光熔覆通过散焦实现较低的稀释率。

3.2.2 组织结构

同一工艺参数下单层、双层和四层熔覆涂层的形貌如图 5(a)、(b)、(c)所示,可见:涂层与基材结合良好,结合处无裂纹、气孔缺陷;三种涂层的生长规律及趋势基本一致,除了厚度有所增加外没有明显的不同。由此可知熔覆层数对涂层微观结构的影响不大。

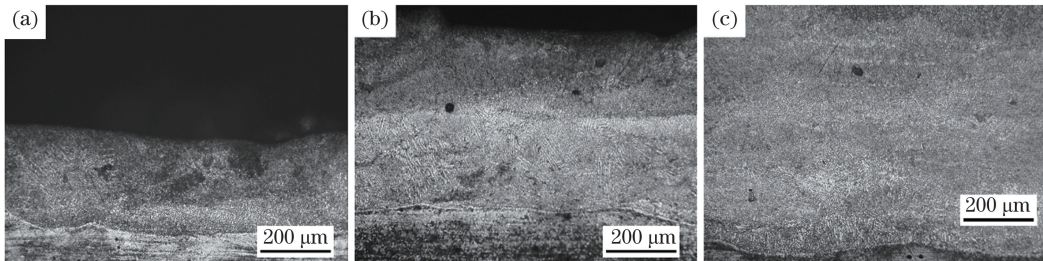


图 5 涂层的形貌。(a)单层涂层;(b)双层涂层;(c)四层涂层

Fig. 5 Morphologies of the cladding coating. (a) Single layer; (b) double layer; (c) four layers

熔覆涂层组织的形核过程与生长形态主要与凝固方向、温度梯度及凝固速率有关,熔覆涂层的整体形貌如图 6(a)所示,涂层与基材结合紧密,孔隙极少。结合 Fe-Cr-Ni 相图^[14]可知,在涂层底部/基体界面处,凝固过程释放的热量都通过基体释放,正温

度梯度下极大的冷速导致结合区以平面晶的方式生长,如图 6(b)所示。随着凝固的持续进行,近结合面处的组织在负温度梯度下沿着散热方向垂直于基体向熔池顶部生长,先析出较为粗大的柱状树枝晶,随着二次枝晶的形成,逐渐在熔覆层中部呈现胞状

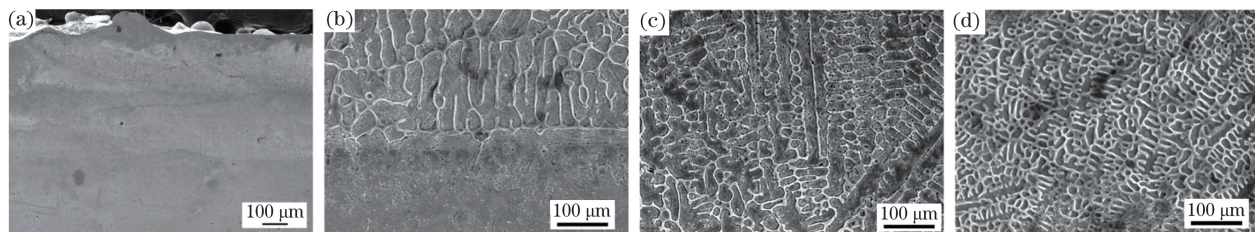


图 6 高速激光熔覆涂层的 SEM 形貌。(a)整体形貌;(b)结合区;(c)中部;(d)近表面

Fig. 6 SEM morphologies of high-speed laser cladding coating. (a) Whole morphology of coating; (b) coating/substrate interface zone; (c) middle zone; (d) near-surface

和外延生长的柱状,如图 6(c)所示。由于高速激光熔覆合金粉末在到达熔池前大部分已为熔融状态,在进入熔池后更加均质,因此近表面的微观结构呈现为细小、均匀的等轴状或树枝状,仅重叠区的枝晶尺寸变得稍粗,如图 6(d)所示。液体在快速结晶过程中先析出 δ 相,获得 $\delta+\gamma$ 共晶成分,随后在一次及二次 γ 枝状晶间隙处形成由 α 相组成的骨架状共析体;在极快的冷却速度下,凝固中后期奥氏体没有发生珠光体转变,而且粉末中的镍导致马氏体转变开始温度(M_s 点)和结束温度(M_f 点)同时降低,因此也没有发生马氏体转变,组织的均匀化比较完全,没有碳化物生成,最终生成只含有 γ 相和 α 相的超

细均质等轴树枝晶,如图 7 所示。

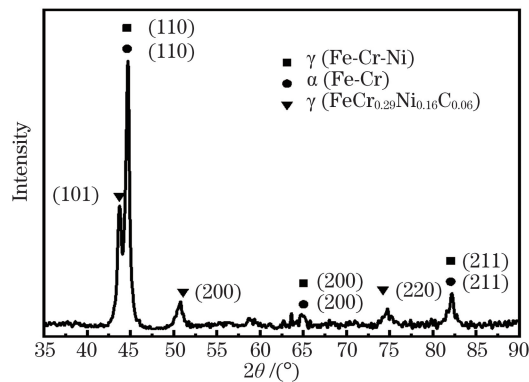


图 7 高速激光熔覆涂层的 XRD 图谱

Fig. 7 XRD pattern of high-speed laser cladding coating

3.2.3 晶粒尺寸

晶粒度可以通过晶粒的平均直径来表征。采用 Nano Measurer 软件和图 8(a)所示的圆截点法分别测量图 6(d)中近表层晶粒的平均直径,软件的测量结果如图 8(b)所示。晶粒粒度级别的计算公式为^[15]

$$G = 6.64385 \lg P_L - 3.288, \quad (2)$$

$$P_L = \frac{M \times P_i}{L}, \quad (3)$$

式中: G 为晶粒的粒度级别; P_L 为 1 倍单位长度(mm)试验线与晶界相交的截点数; P_i 为晶界与试

验线的交点数; M 为所用显微镜的放大倍数。由(2)、(3)式计算可得 $G=14$,查表得高速激光熔覆涂层晶粒的平均直径 $\leq 2.8 \mu\text{m}$,与采用测量软件 Nano Measurer 的统计结果($2.47 \mu\text{m}$)极为接近,相对常规激光熔覆同成分粉末生成的晶粒^[16](直径约为 $6.7 \mu\text{m}$)更为细小。晶粒尺寸的差异主要由冷却速度决定,大的冷却速度使得晶粒形核率提高,抑制了粗大树枝晶的形成。高速激光熔覆的热输入(11.1 kJ/m)远低于同成分粉末在常规激光熔覆工艺^[16]下的热输入(50 kJ/m),超低的热输入和较高的熔覆速度有助于提高冷却速度,因此导致枝晶细化。

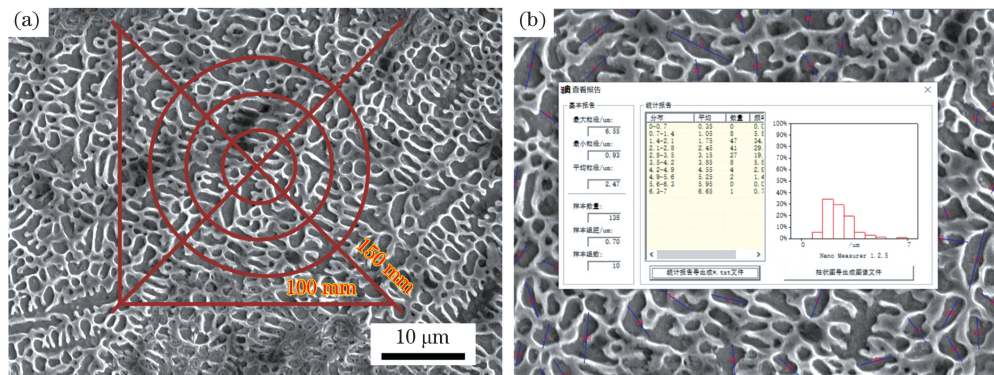


图 8 晶粒平均直径的计算。(a)圆截点法;(b)软件 Nano Measurer 的测量结果

Fig. 8 Calculation of average grain diameter. (a) Single circle grain boundary intersection count; (b) software Nano Measurer's measurements

3.3 高速激光熔覆涂层的显微硬度和耐蚀性

3.3.1 显微硬度

双层涂层横截面的显微硬度如图 9 所示,可见:显微硬度的波动与成分分布趋势大致吻合;在距涂层表面约 $480 \mu\text{m}$ 的范围内,显微硬度基本处于 $650\sim750 \text{ HV0.2}$ 之间,在距表面约 $480 \mu\text{m}$ 时显微硬度发生骤降,至 $550 \mu\text{m}$ 左右时约降至 280 HV0.2 。涂层显微硬度的均值约为 727 HV0.2 ,与电镀硬铬的表面硬度持平^[17],远高于同成分常规激光熔覆^[16]

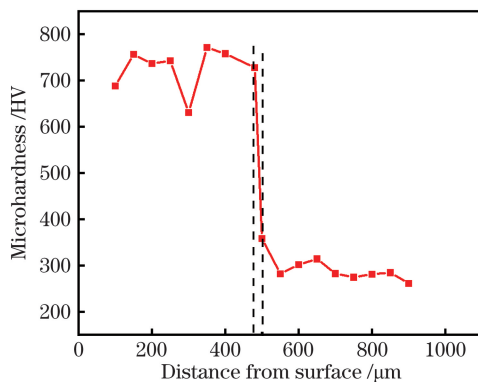


图 9 双层涂层的显微硬度分布

Fig. 9 Microhardness distribution of double-layer coating

涂层(385.98 HV0.2),为基体本身硬度(242.65 HV0.2)的近 3 倍。结合涂层的微观形貌可知硬度的提高主要源于细晶强化作用。

3.3.2 耐蚀性

作为电镀硬铬的替代之一,高速激光熔覆涂层的耐蚀性成为其主要的考核指标之一。极化曲线中的自腐蚀电位反映材料的热力学腐蚀倾向,自腐蚀电位越大,表示材料的腐蚀倾向相对越小;自腐蚀电流密度和腐蚀速率反映材料的均匀腐蚀速率,数值越大表示材料的腐蚀越快。涂层及基体在 3.5% NaCl 溶液(溶液中 NaCl 的质量分数为 3.5%)中的动电位极化曲线如图 10(a)所示。采用 Tafel 外推法确定的自腐蚀电位 E_{corr} 、自腐蚀电流密度 I_{corr} 如表 3 所示。可以看出,虽然涂层和基体的自腐蚀电位相差很小,但涂层的自腐蚀电流密度约为基体 3.3%。涂层表现出典型的钝化行为,且在局部腐蚀开始后电流很快再次趋于稳定,说明涂层的钝化膜具有优异的保护性。

在图 10(b)所示的奈奎斯特图(Z' 表示阻抗的实部, Z'' 表示阻抗的虚部)中,基体和涂层在所选的

频率区域都显示出未完成的半弧,半弧直径越大表示钝化膜的耐蚀性越好,从而进一步证实了涂层的耐蚀性较基体高。在图 10(c)、(d)所示的波特图(Z 表示阻抗, θ 表示阻抗相位角, f 表示正弦波频率)

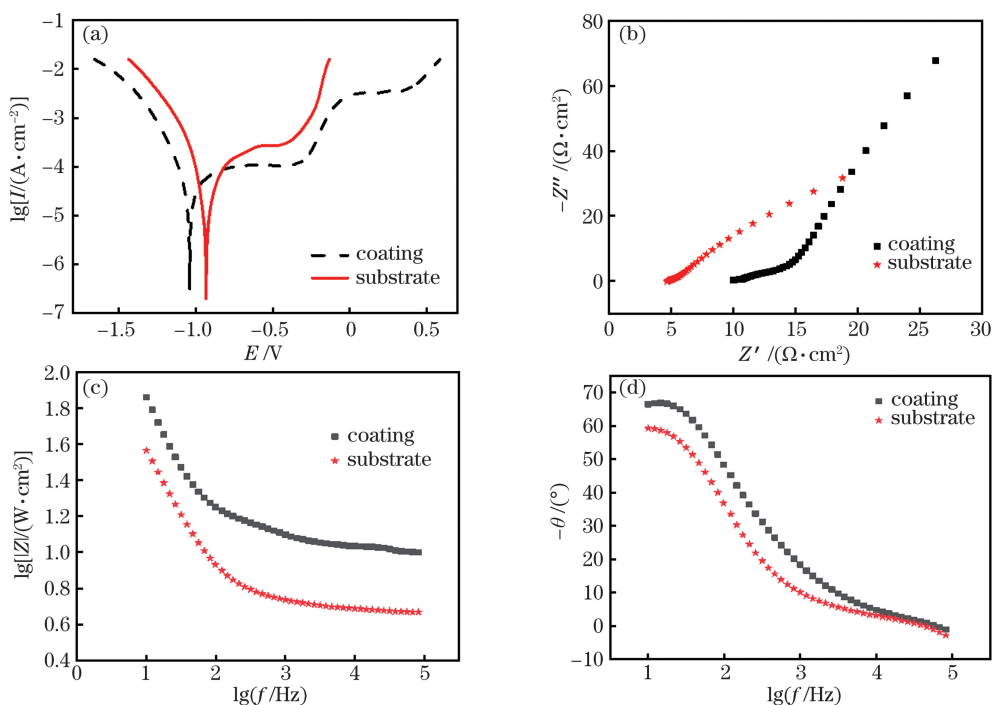


图 10 基体和涂层在 3.5% NaCl 溶液中的耐蚀性。(a) 极化曲线;(b) 奈奎斯特图;(c)(d) 波特图

Fig. 10 Corrosion resistance of substrate and cladding coating in 3.5% NaCl solution. (a) Polarization curves; (b) Nyquist diagram; (c)(d) Bode diagram

表 3 基体和涂层的电化学腐蚀性能

Table 3 Electrochemical corrosion performance of substrate and cladding coating

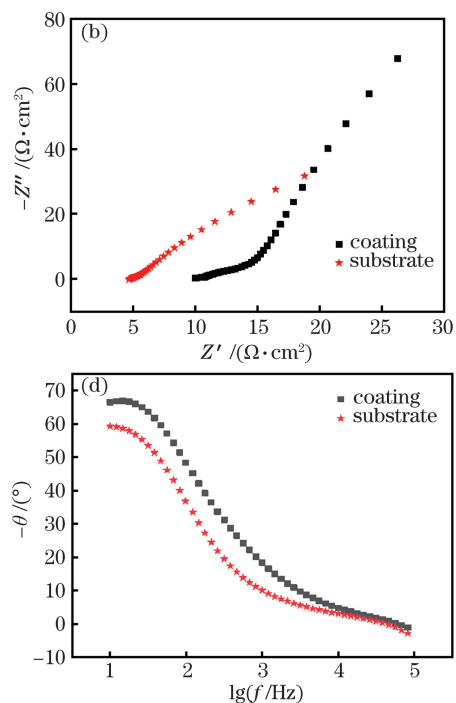
Sample	$E_{\text{corr}}/\text{mV}$	$I_{\text{corr}}/(\mu\text{A} \cdot \text{cm}^{-2})$
Coating	-631.5	0.5267
Substrate	-667	15.9478

涂层的耐蚀性主要取决于晶粒尺寸及其分布的均匀性、钝化薄膜的形成、碳化物含量:高熔覆速度形成的细小、均匀的晶粒可以提高涂层固溶体枝晶间的电位差,减缓腐蚀速度;细小晶粒表面的大量位错可以促进钝化薄膜的成核;在钝化过程中,均匀的粒度分布会加大固溶体中合金元素的固溶度,有助于形成致密的钝化膜并使其保持稳定,阻断基体与腐蚀介质的接触;涂层中无碳化物形成可以保证钝化膜的致密连续。

4 结 论

高速激光熔覆获得的涂层与基体呈冶金结合,涂层的表面粗糙度低、稀释率小;相较于常规激光熔

中可以看出:涂层在中低频段($10^{-3} \sim 10^3 \text{ Hz}$)的极化电阻比基体高,腐蚀速率比基体低;涂层的 θ 值接近 -70° 。所有这些特征都表明涂层在 3.5% NaCl 溶液中形成了稳定的钝化膜^[18]。



覆较为粗大紊乱的枝晶,高速激光熔覆工艺制备的铁基涂层的整体枝晶组织更加细小、晶间成分差异更小、晶粒分布更加均匀。

采用高速激光熔覆工艺制备的铁基涂层在细晶强化和固溶强化的共同作用下具有基体 3 倍的硬度,其自腐蚀电流密度约为基体的 3.3%,耐蚀性能更为优异。

高速激光熔覆获得的涂层无论是表面成形质量、硬度还是耐蚀性都满足镀硬铬涂层的工作条件,高速激光熔覆在提高工作效率的同时减少了后续加工材料和能源的浪费。

参 考 文 献

- [1] Sun H Y, Yang Q, Fan J L, et al. Development status and trend analysis of Xinjiang coal and coal chemical industry [J]. Coal Economic Research, 2020, 40(2): 57-61.
孙海勇, 杨芊, 樊金璐, 等. 新疆煤炭及煤化工产业发展现状与趋势分析 [J]. 煤炭经济研究, 2020, 40(2): 57-61.
- [2] Huang L F, Sun Y N, Wang G J, et al. Research

- progress of laser cladding high-entropy alloy coating [J]. *Laser & Optoelectronics Progress*, 2019, 56(24): 240003.
- 黄留飞, 孙耀宁, 王国建, 等. 激光熔覆技术制备高熵合金涂层研究进展[J]. 激光与光电子学进展, 2019, 56(24): 240003.
- [3] Chen J F, Li X P, Xue Y P, et al. Friction and wear properties of laser cladding Fe901 alloy coating on 45 steel surface[J]. *Chinese Journal of Lasers*, 2019, 46(5): 0502001.
- 陈菊芳, 李小平, 薛亚平, 等. 45钢表面激光熔覆Fe901合金的摩擦磨损性能[J]. 中国激光, 2019, 46(5): 0502001.
- [4] Su L C, Li S, Du X Y, et al. Analysis of hydraulic support column laser cladding remanufacturing performance, economic benefit and environmental benefit[J]. *Inner Mongolia Coal Economy*, 2015(4): 25-27.
- 苏伦昌, 李胜, 杜学芸, 等. 液压支架立柱激光熔覆再制造的性能、经济效益和环境利益分析[J]. 内蒙古煤炭经济, 2015(4): 25-27.
- [5] Raykis O. Alternative with a future: high-speed laser metal deposition replaces hard chrome plating [J]. *Laser Technik Journal*, 2017, 14(1): 28-30.
- [6] Schopphoven T, Gasser A, Backes G, et al. EHLA: extreme high-speed laser material deposition [J]. *Laser Technik Journal*, 2017, 14(4): 26-29.
- [7] Schopphoven T, Gasser A, Wissenbach K, et al. Investigations on ultra-high-speed laser material deposition as alternative for hard chrome plating and thermal spraying[J]. *Journal of Laser Applications*, 2016, 28(2): 022501.
- [8] Wang Y Y, Niu Q, Yang G J, et al. Investigations on corrosion-resistant and wear-resistant coatings environmental-friendly manufactured by a novel super-high efficient laser cladding [J]. *Materials Research and Application*, 2019, 13(3): 165-172.
- 王豫跃, 牛强, 杨冠军, 等. 超高速激光熔覆技术绿色制造耐蚀抗磨涂层[J]. 材料研究与应用, 2019, 13(3): 165-172.
- [9] Lampa C, Smirnov I. High speed laser cladding of an iron based alloy developed for hard chrome replacement [J]. *Journal of Laser Applications*, 2019, 31(2): 022511.
- [10] Li L Q, Shen F M, Zhou Y D, et al. Comparison of microstructure and corrosion resistance of 431 stainless steel coatings prepared by extreme high-speed laser cladding and conventional laser cladding [J]. *Chinese Journal of Lasers*, 2019, 46(10): 1002010.
- 李俐群, 申发明, 周远东, 等. 超高速激光熔覆与常规激光熔覆431不锈钢涂层微观组织和耐蚀性的对比[J]. 中国激光, 2019, 46(10): 1002010.
- [11] Li Y, Bai R X, Lou Y L, et al. Microstructure of ferrous alloy coatings deposited by 1.8 kW high speed laser cladding [C]//Proceedings of the 21st International Thermal Spraying Symposium and the 22nd National Thermal Spraying Annual Conference. [S.l.: s.n.], 2018: 77-82.
- 李岩, 白瑞兴, 娄丽艳, 等. 1.8 kW 高速激光熔覆铁基合金工艺与组织结构[C]//第二十一届国际热喷涂研讨会暨第二十二届全国热喷涂年会论文集. [出版地不详: 出版者不详], 2018: 77-82.
- [12] Li S C, Mo X, Xiao G, et al. The microstructure characteristics and their influence factors during laser additive manufacturing of metal materials[J]. *Laser & Optoelectronics Progress*, 2021, 58(1): 0100007.
- 李时春, 莫彬, 肖罡, 等. 金属材料的激光增材制造微观组织结构特征及其影响因素[J]. 激光与光电子学进展, 2021, 58(1): 0100007.
- [13] General Administration of Quality Supervision Inspection and Quarantine of the People's Republic of China. *Seamless hot-rolled steel tubes for hydraulic pillar service: GB/T 17396—1998* [S]. Beijing: Standards Press of China, 2004.
- 中华人民共和国国家质量监督检验检疫总局. 液压支柱用热轧无缝钢管: GB/T 17396—1998[S]. 北京: 中国标准出版社, 2004.
- [14] Bian S, Zhang Y T, Wang C Z, et al. Phase diagram calculation for Fe-Cr-Ni system [J]. *Journal of Shenyang Ligong University*, 2011, 30(6): 17-21.
- 边书, 张玉妥, 王承志, 等. Fe-Cr-Ni系相图计算[J]. 沈阳理工大学学报, 2011, 30(6): 17-21.
- [15] General Administration of Quality Supervision, Inspection and Quarantine of the People's Republic of China. *Metal-methods for estimating the average grain size: GB/T 6394—2002* [S]. Beijing: Standards Press of China, 2003.
- 中华人民共和国国家质量监督检验检疫总局. 金属平均晶粒度测定法: GB/T 6394—2002[S]. 北京: 中国标准出版社, 2003.
- [16] Fan P F, Sun W L, Zhang G, et al. Microstructure, properties and applications of laser cladding Fe-based alloy gradient coatings[J]. *Materials Reports*, 2019, 33(22): 3806-3810.
- 范鹏飞, 孙文磊, 张冠, 等. 激光熔覆铁基合金梯度涂层的组织性能及应用[J]. 材料导报, 2019, 33(22): 3806-3810.
- [17] He Z M. *Study on chromium electroplating process and properties of fastener surface* [D]. Shenyang: Shenyang University of Technology, 2016.
- 何昭民. 紧固件表面电镀铬工艺及性能研究[D]. 沈阳: 沈阳工业大学, 2016.

- [18] Luo H, Gao S J, Dong C F, et al. Characterization of electrochemical and passive behaviour of Alloy 59 in acid solution [J]. *Electrochimica Acta*, 2014, 135: 412-419.

Microstructure and Properties of Iron-Based Alloys Coatings Prepared by High-Speed Laser Cladding

Xu Yifei¹, Sun Yaoning^{1*}, Wang Guojian¹, Gui Yongliang²

¹College of Mechanical Engineering, Xinjiang University, Urumqi, Xijiang 830047, China;

²College of Metallurgy and Energy, North China University of Science and Technology, Tangshan, Hebei 063210, China

Abstract

Objective With the release of “Energy Planning for the Core Area of the Silk Road Economic Belt” in 2018, Xinjiang’s coal industry is about to enter an unprecedented significant leap-forward development. In the manufacturing industry, it is paramount to develop new coating technologies for wear and corrosion protection of large and high-quality components. The most common process for wear and corrosion protection is hard chromium plating. Its biggest drawback concerns environmental protection. Moreover, the electrochemical processes consume much energy and become less economical as electricity cost increases. Therefore, new alternatives to hard chromium plating are under investigation, and high-speed laser cladding (HSLC) is such an alternative. The benefits of laser cladding (LC) are low heat input, low dilution with the substrate, less material consumption, and overall good performance. HSLC overcomes the efficiency obstacle of conventional LC technology, as well as provides an environmentally friendly and cost-effective production mode for the fabrication of thin coatings on large parts. To meet the tough health and environmental demands along with industries need for lower costs, high-quality iron-based alloy coating material suitable for HSLC was prepared. Through the analysis of its macro-morphology, microstructure, hardness, and corrosion resistance, the basis for improving the corrosion resistance and service life of hydraulic props is provided.

Methods In this study, 45 steel was selected as the substrate. Iron-based alloy powder was used as coating materials. A ZKZM-2000 fiber laser system was employed. A defocus of 15 mm was adopted. The diameter of the beam spot was 1.2 mm. The powders were fed by a powder feeder, and argon was employed as the carrier gas. The main distinctions between HSLC and conventional LC are the melting mode of powder and the formation mode of the molten pool. For the former, the focal planes of the powder stream and laser beam are above the molten pool. Under such conditions, most of the powders are heated and melted before being injected into the molten pool. For the latter, the powders are mainly melted in the molten pool. At 50% overlapping rate, 260 μm thickness and $\sim 7.1\%$ dilution rate of the coating can be obtained. Macroscopic features and microhardness were investigated using an ultra-depth three-dimensional microscope and a microhardness tester, respectively. Test specimens were etched using aqua regia to analyze the microstructure and phase components of the coatings using scanning electron microscopy, energy dispersive spectrometry, and X-ray diffractometry (XRD). The corrosion behavior of the coating was evaluated using CHI660E system at room temperature (20 °C). The medium was 3.5% NaCl solution.

Results and Discussions The cladding efficiency of the HSLC process could reach up to 0.243 m^2/h . Under the same process parameters, the growth laws and trends of single-layer, double-layer, and four-layer coatings are basically the same, indicating that the increase in the number of cladding layers has little effect on the microstructure of the coating. The HSLC samples were formed uniformly at the macro-level, and the surface roughness was controlled at 21.38 μm , which was less than 10% of the conventional LC samples (Fig. 2). The geometric dilution ratio is $\sim 7.1\%$, which is uniform and dense, in addition to good metallurgical bonding to the substrate. The low dilution ratio obtained from the HSLC process is due to low heat input and specific metallurgical forms. The result of the XRD pattern for HSLC coating indicates that the coating mainly consists of α and γ phases (Fig. 7). The ultrafine dendrites with an average grain diameter of less than 2.8 μm are formed (Fig. 6). The difference between grain sizes is mainly determined by the cooling rate. High cladding speed contributes to increasing cooling rate, which causes low dilution ratio and dendrites refinement. The microhardness of the coating is about three times as high as

the substrate. In a 3.5% NaCl solution, the corrosion current of the coating dropped by two magnitudes compared to substrate, which indicates that a more uniform microstructure of HSLC coatings leads to a higher corrosion resistance.

Conclusions Cladding layers of iron-based alloy powders were prepared on 45 steel surface using HSLC. The macroscopic features, microstructure, and corrosion resistance were comparatively investigated. The crack-free layers obtained with HSLC present good metallurgical bonding with the substrate and a high degree of uniformity and compactness. At a scanning speed of 3600 mm/min, the coating thickness is up to 260 μm , with a dilution rate of $\sim 7.1\%$. Compared with the dendrite characteristics by messy dendrites of the conventional LC, the microstructure of the coating prepared by HSLC is mostly dendrites. Moreover, its microstructure of dendrite is finer, the difference in composition between grains is smaller, and the distribution of grains is more uniform. The microhardness of the HSLC coating is three times as high as the substrate under the joint action of grain refinement and solid solution strengthening. The corrosion behavior in 3.5% NaCl solution indicates that the HSLC coating has good corrosion resistance, and its corrosion current density I_{corr} is two and three orders of magnitude lower than that of conventional LC coating and hard chromium plating, respectively. Therefore, the coating obtained from HSLC can satisfy the tough health and environmental demands. In addition to improving the work efficiency, the waste of follow-up processing materials and resources is reduced.

Key words laser technique; high-speed laser cladding; iron-based alloy; chromium electroplating; corrosion resistant coating

OCIS codes 140.3390; 160.3900; 350.3390